Review Vol. 12, No. 1 / 1 Jan 2022 / Optical Materials Express 256
Optical Materials EXPRESS

Vacuum-evaporated lead halide perovskite LEDs [Invited]

FEI YAN[1] AND HILMI VOLKAN DEMIR[1,2,3,*]

[1]LUMINOUS! Centre of Excellence for Semiconductor Lighting and Displays, TPI-The Photonics Institute, School of Electrical and Electronic Engineering, Nanyang Technological University, 639798, Singapore
[2]Division of Physics and Applied Physics, School of Physical and Mathematical Sciences, Nanyang Technological University, 639798, Singapore
[3]Department of Electrical and Electronics Engineering, Department of Physics, UNAM–Institute of Materials Science and Nanotechnology, Bilkent University, Ankara 06800, Turkey
*HVDEMIR@ntu.edu.sg

Abstract: Lead halide perovskites (LHPs) have made impressive progress in solid-state optoelectronics by virtue of their excellent electronic and optical features. In the past few years, the light-emitting diode (LED) adopting LHP emitters have reached a comparable level of external quantum efficiency (EQE) with organic and colloidal quantum dot LED counterparts. Apart from solution-processing, all-inorganic $CsPbX_3$ LEDs can also be fabricated using thermal evaporation in a single run without breaking vacuum. In principle, all-evaporated LHP-LEDs in a vacuum demonstrate good uniformity and reliability in a large-area, especially full color applications where color pixelation is necessary, although their performance is still lower than that of the devices using hybrid film depositions. Herein, the understanding of vacuum-evaporated LHPs and their resulting LEDs, including the materials, film deposition and device issues, are reviewed. Additionally, guidelines toward high-performance devices and their prospects in the future are included.

1. Introduction

As new generation of semiconductor materials, the lead halide perovskite (LHP) family has proven their worth in optoelectronics, especially in light-emitting diodes (LEDs), by virtue of the achievements reached in the past few years [1–20]. Compared to their counterparts, namely, organic LEDs (OLEDs) and semiconductor colloidal quantum dot LEDs (QD-LEDs), LHP-LEDs demonstrate a competitive or even a higher level of performance, including their high brightness, high external quantum efficiency (EQE) and ultra-wide color gamut [1–13,18–22]. Generally, the LHP emissive layer is deposited onto a substrate by solution-processing, in principle, which is supposed to be an advantageous for low manufacturing costs [1–13,18–20,23]. As a new generation of fantastic display technologies, the impressive progress of LHP-LEDs achieved in the laboratory means that industry-scale manufacturing in the next few years is critical because of the intensive homogenization competition from OLEDs, QD-LEDs and other emerging display technologies. However, solution-processing also plays an insurmountable role in hindering the further improvement of LHP-LEDs whose structural design and fabrication were severely restricted by the orthogonal selection of solvents [24–27]. Almost all the so-called solution-processed LHP-LEDs, especially high-performance LHP-LEDs, still require a high vacuum chamber for the deposition of subsequent functional layers [1–13,19,20,23]. Thus far, most device research actually concentrates on the emissive materials and their film deposition. An industry-scale LED display always requires that all pixels have a super-high uniformity over a large area, which is still a challenge for laboratory-scale solution-processing as a film deposition technology.

#442770 https://doi.org/10.1364/OME.442770
Journal © 2022 Received 10 Sep 2021; revised 10 Nov 2021; accepted 11 Nov 2021; published 22 Dec 2021

Optical Materials EXPRESS

Fortunately, apart from solution processing, some LHPs can also be deposited using thermal evaporation in a vacuum chamber, which means good compatibility with the well-established all-evaporated LED industry [28–34]. The vacuum-evaporated LHP emissive films have an innate advantage in their uniformity of a large-area film, which is essential for LED displays. Among all LHPs, all-inorganic $CsPbX_3$, especially $CsPbBr_3$, demonstrated the best thermal evaporation in vacuum and is thereafter the main covering material in this review [19,28–32,34]. All-inorganic $CsPbBr_3$ demonstrates some special features that differ from other LHP family members, for instance, the high thermal stability of all-inorganic $CsPbX_3$ make it a candidate for high driving-current, high brightness LEDs and even laser diodes and other current-driven applications in the future [35–37]. In the past few years, vacuum-evaporated $CsPbBr_3$ emissive films have achieved impressive progress in LEDs; however, these films are still dominated by solution-processed counterparts [28–34,38,39]. Statistically, the performance of LEDs containing a vacuum-evaporated $CsPbBr_3$ emissive layer still falls far behind that of devices with a solution-processed $CsPbBr_3$ emissive layer. (Table 1)

Table 1. Comparison of the key performance of LEDs with a LHP emissive layer deposited using vacuum-evaporation and solution-processing [22, 40, 41].

Comparison	VACUUM-EVAPORATED			SOLUTION-PROCESSED		
	Performance	Structure	Ref.	Performance	Structure	Ref.
L_{max} (cd m^{-2})	15 745 cd m^{-2}	ITO/PEDOT:PSS/ /LHP//EABr/TPBi/PT-T2T/Li/Al	[38]	496 320 cd m^{-2}	ITO/a-ZSO/LHP/NPD/MoOx/Ag	[40]
EQE_{max} (%)	8.86 %	ITO/PEDOT:PSS/ /LHP//EABr/TPBi/PT-T2T/Li/Al	[38]	21.63 %	ITO/PEDOT:PSS/PTAA/LHP/TPBi/PT-T2T/Li/Al	[22]
Area (mm^2)	4020 mm^2	ITO/NiOx/LHP/TPBi/ LiF/Al	[39]	5400 mm^2	ITO/poly-TPD/LHP/TPBi/LiF /Al	[41]

In this review, some up-to-date progress achieved in the LEDs using a vacuum-evaporated LHP emissive layer, especially $CsPbBr_3$, is provided. Insights into the film deposition, device structure design and fabrication, and guidelines for high-performance vacuum-evaporated LHP-LEDs are presented. This review can possibly trigger subsequent studies or new possibilities in LHP-LEDs and other related subfields.

2. Fundamental properties of LHPs for LEDs

In general, LHPs are typical ionic compounds that can be expressed as $(R)_2(A)_{n-1}B_nX_{3n+1}$, where site A is a monovalent cation, e.g., formamidinium (FA^+), methylammonium (MA^+), Cs^+ and their combination; site B is Pb^{2+}; and site X is Cl^-, Br^-, I^- and their combination [42–46]. In the LHP crystal structure, the $[PbX_6]^{4-}$ octahedron formed by halogen anions is the core fragment, and the pivot site is always Pb^{2+}. When n=1, a monolayer corner-sharing $[PbX_6]^{4-}$ octahedral forms a 2D perovskite sheet that is sandwiched by two organic ligand layers (R) (Fig. 1(a)) [43,44,47]. As the n value increases, the formula can be simplified to $APbX_3$, which

Optical Materials EXPRESS

corresponds to classical 3D LHPs (Fig. 1(a)) [43,45,47]. LHPs deposited in a vacuum chamber by thermal evaporation are generally 3D crystalline structures based on elemental corner-sharing $[PbX_6]^{4-}$ octahedra because there is no symmetry breaking factor. For example, the molecular spacers used in solution-proceeded 2D LHPs can block the assembly of elemental corner-sharing $[PbX_6]^{4-}$ octahedra out of plane [48].

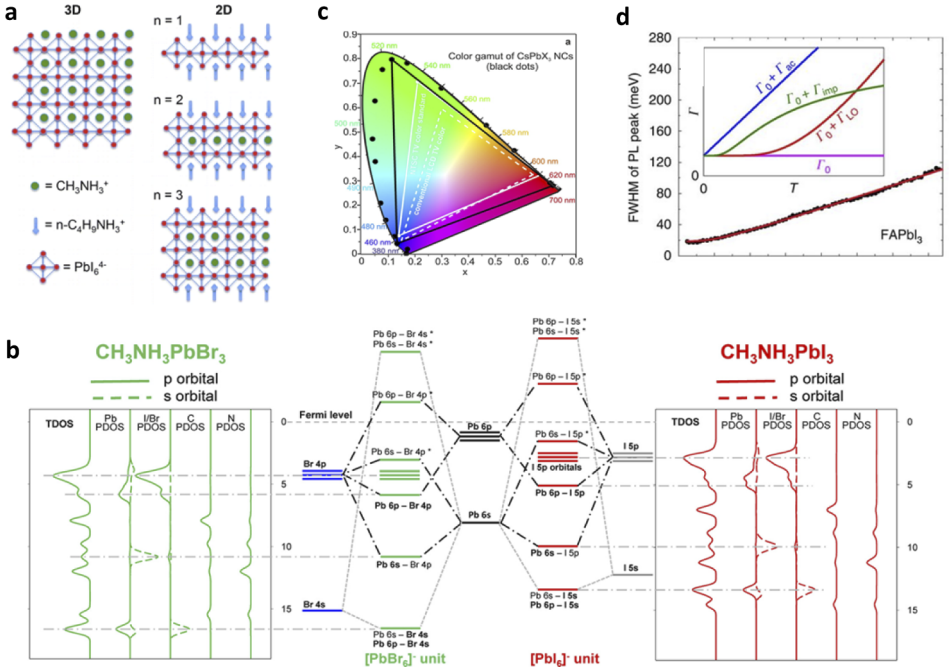

Fig. 1. (a) Schematic of 3D and quasi-2D lead halide perovskites. Reproduced with permission [47] Copyright © 2015 American Chemical Society. (b) Schematic energy diagram of lead halide perovskites and their corresponding total density of states (TDOS) and the partial density of states (PDOS). Reproduced with permission [49] Copyright © 2017 American Chemical Society. (c) CIE chromaticity coordinates comparison among $CsPbX_3$ NCs (dark points), the consumer LCD TVs (dashed white line) and the color standards of TVs (NTSC) (solid white line). Reproduced with permission [50] Copyright © 2017 American Association for the Advancement of Science. (d) The dependence of PL linewidth of $FAPbI_3$ on temperature. Reproduced with permission [51] Copyright © 2016 The Author(s).

The energy diagram of emitters is a very important factor for the resulting LEDs because the related bandgap and states will influence the optical properties, and the energy level position of the conductive band (CV) and valence band (VB) will determine the charge carrier injection and selection of matched functional layers. The energy diagrams of LHPs are mainly determined by the orbital hybridization of lead and halogen (Fig. 1(b)) [11,49,52–54]. Regarding CB, the Pb-6p orbitals play a primary role compared to the slight contribution of the np orbitals of halogens (Cl-3p, Br-4p, I-5p) (Fig. 1(b)) [49,55]. In contrast, in the VB, which is hybridized by the X-*n*p orbitals and the Pb-*6*s orbitals, the contribution of halogens is higher; thus, the energy level of VB and the resulting band gap can be widely tuned by adopting different halogen species (Fig. 1(b)) [49,54,56]. In addition to the single halogen species $CsPbCl_3$, $CsPbBr_3$ and $CsPbI_3$ with a fixed band gap, alloyed halide species can also take site X to form $CsPbCl_xBr_yI_z$ (x + y+z=3) [55,57]. By changing the ratio of halogen species, the band gap can be tuned over 1 eV; correspondingly, the light emission shifts continuously from the near-infrared to the near-ultraviolet [11,58–60].

Optical Materials EXPRESS

Along with their narrow linewidth, the LHP family demonstrates an ultrawide color gamut over the NSTC standards, which can reappear as almost all natural color in their resulting 'true' color displays (Fig. 1(c)) [50,61,62]. The strong polar X-Pb bond in LHPs leads to a Fröhlich coupling between charge carriers and longitudinal optical phonons, which is supposed to be the predominant role in determining the linewidth broadening at room temperature [51,63,64]. In comparison, other factors play minor roles in linewidth broadening. This is the reason for bulky LHPs and their nanocrystalline counterparts to demonstrate comparable linewidths and shapes of emissive spectra (Fig. 1(d)) [51–53,63,65,66]. In a vacuum-evaporated LHP film, the emissive spectra are almost the same.

The most attractive feature of LHPs, unlike typical semiconductors, is their high defect tolerance in light generation. Mostly, the bandgap of normal semiconductors is the energy difference from the top of the bonding VB to the bottom of the antibonding CB. In contrast, both the VB and CB of LHPs are antibonding (Fig. 1(b)) [67,68]. Antibonding means a raised VB maximum, even lying above the level of the X-np and Pb-6s orbitals. Defect states therefore lie within the VB [68,69]. Thus, these tolerated defects do not lead to any significant influence of the interband electron transition and resulting light generation [49,52,53,65,70,71]. However, there are still some extrinsic deep defect states caused by vacancies, halide interstitials and others [72,73]. In the LHPs deposited using vacuum thermal evaporation, there are more defects because of the excess precursors, by-products and grain boundaries during the deposition compared to solution-proceeded LHP NCs with the passivation of ligands [32,74].

In the LHPs deposited using thermal evaporation in vacuum, they are polycrystalline; thus, without any effect of spatial confinement, the LHP excitons are normally Wanier-Mott type with a low binding energy down to dozens of meV [34,55,76,77]. These excitons have a high possibility of dissociating into free charges compared to the radiative recombination [78,79]. Because of the low overlap of wavefunctions between holes and electrons and their high mobilities, radiative recombination is a slow second-order bimolecular process (Fig. 2(a)) [6,75,80,81]. The many defects formed during the thermal evaporation also make a significant contribution to the consumption of excitons by a prompt first-order trap mediated non-radiative recombination [6,75,80–82]. Because of the low exciton binding energy, in LHP-LEDs the applied external electric field provides an additional pathway of consuming excitons by dissociating them into free-charge carriers [83,84]. Therefore, an effective enhancement of the crystalline quality of deposited LHPs, along with charge carrier confinement, is required for highly efficient light emission.

Differing from the optically-excited applications, as a current-driven structure, good electric properties are essential for LEDs [18–20]. LHPs demonstrate superior charge carrier transport features, including ambipolar character, high mobility up to thousands of $cm^2\ V^{-1}s^{-1}$ and long lifetime charge carries [51,85–87]. The charge carrier flows through the 3D LHPs as a large polaron with radii lager than 40-50 Å, which exceeds the lattice constant and is immune from scattering with defects, other carriers, and even phonons [88–90]. Comparable hole and electron mobilities are supposed to be important merits for LHP-LEDs, which always requires balanced hole and electron injection [6,90,91]. In addition, intrinsic ion migration also makes a nonnegligible contribution to charge transport, which can be observed as hysteresis dependence of driving voltage and current [27,60,84,92]. Although this feature can be used to heal some defects and lower energy barrier for charge carrier injection, it still inevitably leads to concerns about the device stability of LHP-LEDs [93–97]. The VB of LHPs is deep and can be adjusted over 1 eV by changing halogen species, which makes the hole injection difficult, especially the blue-emitting ones (Fig. 2(b)) [49,56]. Thus, it is challenging to find matched hole transport materials with deep HOMO level, especially semiconductive polymer films, which require an additional passivation treatment before the solution-based deposition of LHPs [6,7,17,98].

Optical Materials EXPRESS

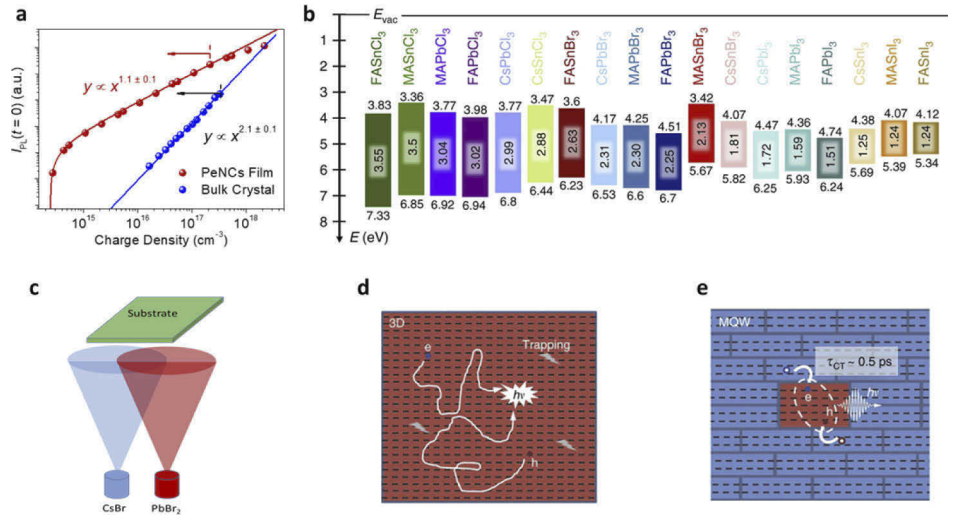

Fig. 2. (a) Initial time PL intensity ($I_{PL}(t = 0)$) as a function of the charge carrier density in PL. Reproduced with permission [6] Copyright © 2018 American Chemical Society. (b) Schematic energy diagram of metal halide perovskites. Reproduced with permission [56] Copyright © 2019 The Author(s). (c) Schematic diagram of $CsPbBr_3$ deposition using vacuum thermal evaporation. (d) Schematic illustration of slow bimolecular recombination. Reproduced with permission [75] Copyright © 2017 The Author(s). (e) Schematic illustration of charge carrier confinement and subsequent recombination in the perovskite multiple quantum wells. Reproduced with permission [75] Copyright © 2017 The Author(s).

3. Vacuum evaporation of LHPs

The vacuum evaporation techniques for thin-film deposition include thermal evaporation, electron beam evaporation, sputtering, molecular beam epitaxy, atomic layer deposition and others. With the consideration of the comparable device structures and fabrication of OLEDs, QD-LEDs and LHP-LEDs and the common functional materials they shared, until now, the vacuum thermal evaporation is the most commonly used technique in the LHP-LED fabrication. In principle, most members of the LHP family can be thermally evaporated [29,48,74,99,100]. Until now, most thermally evaporated LHP films have been used as absorbers in solar cells [99–102]. Organic-inorganic hybrid LHPs are not good candidate materials for vacuum thermal evaporation because of their lower thermal stability in vacuum, which will degrade rather than evaporate with heating [103,104]. For multisource co-evaporation, the organometallic precursors, especially MABr, are difficult to handle because of their high vapor pressure, and a serious contamination will occur [105–107]. In comparison, all-inorganic LHPs and their precursors demonstrate much better thermal evaporation in vacuum, and their films can be deposited by different thermal evaporation scenarios [28,34,74,96]. The $CsPbX_3$ can be deposited by multisource co-evaporation or the subsequent evaporation of the two precursors CsX and PbX_2 [28–30,32,74]. Additionally, it can also be deposited by the single-source evaporation of presynthesized raw $CsPbX_3$ [34,108]. For both scenarios, most deposited $CsPbX_3$ will be subjected to posttreatment for healing defects [28–30,32,34,74]. Normally, thermal annealing and solvent vapour annealing are effective treatments for enhancing the crystal quality of a deposited LHP film [28–30,32,34,74]. Moreover, some additives, especially ion liquids, have also demonstrated great defect elimination capability [109,110].

Optical Materials EXPRESS

3.1. Multisource evaporation

All-inorganic LHPs can be deposited by alternately evaporating two precursors, CsX and PbX_2 (Fig. 2(c)) [28–30,32,74]. By virtue of high ion migration, the heterointerface between two adjacent CsBr and $PbBr_2$ layers will be blurred and even disappear to produce $CsPbBr_3$ domains [29,74,84]. However, the ratio of the two precursors is difficult to handle in this operation. The two precursors can also form other LHP species with different stoichiometric ratios, such as $CsPb_2Br_5$ and Cs_4PbBr_6 [30,74,111]. Therefore, the deposited film could lead to a blend of several LHP species and excess precursors rather than the high purity $CsPbBr_3$. Clearly, these by-products and excess precursor impurities will result in many defects, which leads to a low level of luminous efficiency of the LHP film and their resulting LEDs [30,74,111]. Moreover, this nonuniform emissive film contains different domains of LHP specie domains, which will make the charge carrier transport mechanism more complicated, resulting in an even worse device performance [30,74,111].

Alternatively, the $CsPbBr_3$ film can be deposited by simultaneous co-evaporation of two precursors CsBr and $PbBr_2$ in vacuum [28,48,99]. These two precursors would mix uniformly at the nanoscale during film deposition, and their ratio can be controlled in real time by adjusting the evaporation rate of each precursor. Similarly, two or more different PbX_2 precursors can also be simultaneously co-evaporated with CsX to deposit alloyed halide perovskite films [112]. In principle, the film deposited using this scenario should demonstrate an improved film uniformity. However, on the practical level, precise control of the ratio among different precursors by adjusting the corresponding evaporation rate is difficult over the whole duration of LHP film deposition. Thus, it is still a major challenge to obtain a highly crystalline structure of deposited LHPs. In solution-processed film deposition, precursors will spontaneously react with others with a precise stoichiometric ratio, and in this dynamic growth process, excess reactants will be removed easily by the solvent [113,114]. However, in vacuum thermal evaporation, the excess precursors deposited onto the substrate cannot be removed without any assistance, which will exist as impurities or form other LHP species such as Cs_4PbX_6 [30,74,111].

3.2. Single-source evaporation

In addition to the multisource co-evaporation of precursors, the emissive films can also be deposited by the single-source evaporation of presynthesized $CsPbX_3$ in high vacuum, which can fix the stoichiometry problem [34,108]. In comparison to organic-inorganic hybrid LHPs, all-inorganic $CsPbX_3$ exhibits great thermal stability, making it more suitable for thermal evaporation [35–37]. This good thermal stability depends on the vacuum atmosphere [36]. At a low vacuum level, $CsPbBr_3$ will decompose instead of evaporating, and at a high vacuum level of 10^{-5} Pa, the perovskite structure of $CsPbBr_3$ remains stable with increasing temperature until melting and then evaporating [115–119]. However, it has been reported that at high temperature, highly activated ion migration will lead to some CsBr-rich and $PbBr_2$-rich domains before the evaporation [34]. Therefore, at the macroscale, the deposited film still follows the stoichiometry of $CsPbBr_3$; however, their microscopic perovskite crystal structure is lost. Based on the identical feature of ion migration, after posttreatment, all by-products will convert back to $CsPbBr_3$ [34,36,120]. It has been observed through in situ high-resolution TEM that the crystal structure of $CSPbBr_3$ is destroyed at a high temperature (over 800 °C) and then recovers completely as the temperature is decreased [36].

The vacuum-evaporated emissive films are polycrystalline and contain many $CsPbBr_3$ and other LHP species grains, whose boundaries and impurities would mediate a prompt nonradiative recombination of excitons as trap states [34,65,70,82]. Due to the high defect tolerance, these LHP films still demonstrate a high level of light emission [28–34,52]. However, even if the deposited $CsPbBr_3$ film is a perfect single crystal without any defects, it is still difficult to obtain efficient light emission as high as that of the nanocrystalline emitter counterparts used in

Optical Materials EXPRESS

LEDs. Because of the negligible wavefunction overlap of electrons and holes, there is a small chance that opposite charge carriers will meet each other, which means a low-efficiency radiative recombination for LEDs (Fig. 2(d)) [6,75,80,81]. Thus, the LHP-LEDs are dominated by LHP nanocrystals, quantum dots, quantum wells, nanoplatelets and other nanostructures that confine electrons and holes in a small domain with dimensions of nanometers to facilitate their radiative recombination (Fig. 2(e)) [1–17]. Without effective charge carrier confinement, sufficient exciton binding energy and effective passivation of surface defects, it is difficult to further improve the light emission to a comparable level of solution-processed LHP NCs [1–17,28–33,75,80,81].

3.3. Role of the substrate

In most crystal growth, the substrate plays an important, even a critical-level role. The LHP vapour deposits onto an organic semiconductor substrate to form a solid thin film, which is also a crystallization process; thus the role played by organic semiconductor substrate during the crystal growth is considerable. Until now, there are still a few works focusing onto this topic [99,121]. The surface potential of organic substrate was proved to play an important role in the crystallization during the solution-processed film deposition [122,123]. A solution-processed LHP film deposited on top of a hydrophilic PEDOT:PSS substrate demonstrated a smaller grain compared to hydrophobic substrates [122,123]. In the vacuum-evaporated LHPs, the role of organic semiconductor substrate played in film deposition is still a complicated issue. Different organic semiconductor substrates show significant variety in LHP film composition and morphology [99,121]. It is confirmed that without the orthorhombic limitation of solvent, the substrate selection and the device structure design of the whole LHP-LED are more flexible.

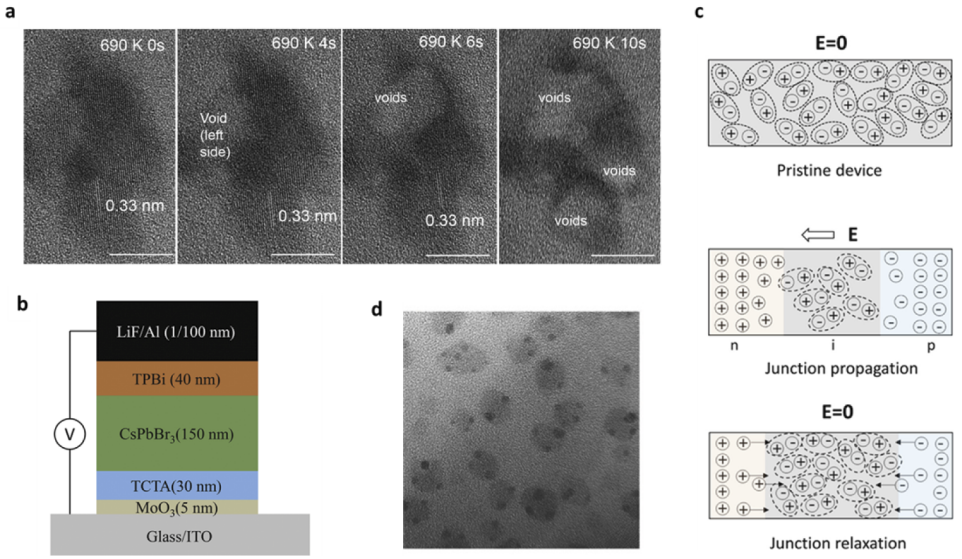

Fig. 3. (a) In situ TEM image of $CsPbBr_3$ nanocrystal in high vacuum (1.2×10^{-5} Pa). Consecutive clip images at 690 K from 0 to 10 s. Scale bars: 10 nm. Reproduced with permission [36] Copyright © 2019 Author(s). (b) Schematic device architecture of the all-vacuum-evaporated perovskite LEDs. Reproduced with permission [33] Copyright © 2020 Author(s). (c) Schematic of doping effect at the interface caused by ion migration under applied electric field. Reproduced with permission [124] Copyright © 2018 American Chemical Society. (d) TEM image of $CsPbBr_3$ nanocrystals embedded Cs_4PbBr_6 matrix. Reproduced with permission [125] Copyright © 2018 The Authors.

Optical Materials EXPRESS

The complicated influences on organic semiconductor substrate caused by the subsequent solution-processing onto it are also eliminated completely.

3.4. In situ treatment and post treatment of LHP films

In single-source vacuum thermal evaporation, the macroscale-ordered structure of $CsPbBr_3$ will be destroyed, and the vapor should be a nanoscale cluster of $CsPbBr_3$ (Fig. 3(a)). Because of the enhanced ion migration at high temperature, some CsBr-rich and $PbBr_2$-rich domains form in the raw $CsPbBr_3$ [34]. The deposited LHP grains are much smaller than the solution-processed grains, which means more boundaries [126]. Thus, a treatment is required to improve the crystal quality of the deposited LHPs. Thermal annealing is a simple and effective post-treatment for enhancing the crystalline quality of the deposited $CsPbBr_3$ film [48,100,127]. However, if the annealing temperature is too high, the deposited $CsPbBr_3$ films will lose their light emission [34]. It is noted that there is a significant discrepancy about whether thermal annealing can enhance the light emission of a vacuum-evaporated $CsPbBr_3$ film, which means that there is still an unknown mechanism about the crystallization of LHP during thermal evaporation that needs to be uncovered [34,48]. In situ temperature management of substrate was proved to make a significant influence on the size of the deposited LHP crystal [121]. As decreasing temperature from room temperature to -2 °C, the deposited LHP grain size increases from 100 nm to micrometer level [121]. In addition, solvent vapor annealing, ion liquid additives and precursors like PEABr were also used to heal the defects of deposited LHP [74,100]. Until now, most treatment works still concentrated onto the LHP absorber in solar cells.

4. LEDs exploiting vacuum-evaporated LHP emitters

In a sense, solution-processed LHP-LEDs can be considered as a derivative of LHP photovoltaics and QD-LEDs, which share almost the same device structure, even identical functional layers (Fig. 3(b)) [1–17,128]. Similarly, vacuum-evaporated LHP-LEDs also adopt the device structure frame of solution-processed ones, including the ITO anode modification layer of PEDOT:PSS and a semiconductor polymer hole transport layer [28–34]. A highly conductive PEDOT:PSS film is an excellent ITO anode modification layer used in a variety of thin-film optoelectronic applications [74]. Generally, a semiconductor polymer hole transport layer, such as poly-TPD and PVK, is believed to work as an energy steppingstone to facilitate the injection of holes into the LHP emissive layer [28]. Because of the metallic feature, PEDOT:PSS is supposed to be an exciton quencher of the adhesive emissive layer and the semiconductor polymer hole transport layer also worked as a buffer layer for eliminating the quenching of LHPs [129,130]. However, without any semiconductor polymer hole transport layer between the PEDOT:PSS and LHP layers, some LHP-LEDs still demonstrate high brightness, low driving voltages and high EQEs [30,34,74]. Because of the high ion migration of LHPs, a p-type doping layer will be formed at the PEDOP:PSS/LHP interface facilitated by external bias in LEDs [84,124,131,132]. This p-type doping layer will effectively decrease the hole injection barrier from PEDOT:PSS into LHPs, leading to a low driving voltage, although their VB is much deeper than the Fermi level of PEDOP:PSS (Fig. 3(c)) [84,124,131,132]. On the contrary, in some LHP-LEDs using a vacuum-evaporated $CsPbBr_3$ emissive layer deposited onto a PEDOT:PSS film, the driving voltage is much higher, and the origin is probably the low conductivity of by-product Cs_4PbBr_6 [30,74,111].

To achieve highly efficient LHP-LEDs, balanced charge carrier injection is essential. To balance superior hole injection, efficient electron injection is required. For the cathode side, a small molecular electron transport layer, an electron injection or interfacial buffer layer and a thin-film metal cathode were used [28–34]. Because the CB of LHPs is deep, most organic electron transport materials can match the energy level alignment for barrier-free electron injection well [11,49,52–54,56]. However, the electron mobility of most organic electron transport materials is

Optical Materials EXPRESS

orders of magnitude lower than that of LHPs [6]. Using n-type doping, the conductivity of the electron transport layer can be enhanced significantly [133,134]. However, small-size n-type dopants such as lithium, cesium and compound Cs_2CO_3 would diffuse into the emissive layer [135,136]. Whether these hot atoms and ions heal or damage the crystal structure of the deposited LHPs is still unknown. To replace Cs and Cs_2CO_3, some organic n-type dopants like Lewis acids can be used for LHP-LEDs. Moreover, the evaporation temperatures of this kind of inorganic n-type dopant, LiF interfacial buffer layer and metal electrode film are much higher than those of other materials, which would lead to thermal annealing of the deposited LHPs.

Alternatively, some inverted structures were adopted in solution-processed LHP-LEDs, which can fix the unmatched electron injection. There are a few electron transport polymers that can be used in inverted structure LHP-LEDs, the most used electron transport layer is a solution-processed ZnO nanocrystal film on an ITO cathode substrate [137–140]. To modify the energy level alignment and eliminate potential quenching caused by ZnO, an ultrathin PEIE film is used before LHP film deposition [139,140]. Subsequently, an organic hole transport layer CBP and hole injection layer MoO_3 are evaporated [140,141]. To prevent the high temperature from evaporating MoO_3, an organic p-type dopant F4-TCNQ or HAT-CN can be used for efficient hole injection, which can be evaporated at a much lower temperature [136]. Thus far, there are still no vacuum-evaporated LHP-LEDs using an inverted structure.

For most LHP-LEDs using a vacuum-evaporated emissive layer, solution-processed deposition of other functional layers was still used, which abandoned some advantages of the vacuum-evaporated LHPs in LEDs [28–34]. The energy level of different LHPs can be tuned to over 1 eV by using different halogen species [56]. To date, only a few semiconductor polymer candidates can be used in solution-processed LEDs; however, the orthorhombic issue is a further limitation [1–17]. Thus, on the practical level, it is difficult to determine the optimized device structure for all, even only one, LHP species emitter in LEDs. All-evaporated LHP-LEDs in a single run without breaking vacuum may be an option for further improvement of the device performance because of their good reliability and reproducibility. Without the limitation of solution processing in device fabrication, the device structure design, the selection of matched functional layers and reliability control of all-evaporated LHP-LEDs in vacuum are easy to handle. However, until now, only a few all-evaporated devices in vacuum have been reported, and their performance is still far behind that of the devices using a solution-processed LHP emissive layer [29,119].

5. Summary and future prospects

Vacuum-evaporated LHPs have achieved impressive progress in solar cells; however, they are still dominated by their solution-processed counterparts in LEDs. In principle, the area of LHP-LED panel fabricated using vacuum thermal evaporation can reach a comparable level of commercial OLED displays, though most current research works still focus on small-area devices. Among all LHP family members, all-inorganic $CsPbX_3$ is more suitable for vacuum thermal evaporation; $CsPbBr_3$ is the most intensively studied emitter used for LEDs; and the maximum brightness and EQE can reach 15,745 cd m^{-2} and 8.86%, respectively [38]. For the vacuum-evaporated LHP-LEDs, the predominant consideration is the deposition of highly efficient LHP emissive layer. The $CsPbBr_3$ film can be deposited by using the sequential evaporation or co-evaporation of two precursors of CsBr and $PbBr_2$; however, their molar ratio is difficult to handle to obtain a stoichiometric $CsPbBr_3$ during the whole deposition process. Alternatively, pre-synthesized $CsPbBr_3$ can be directly evaporated as the emissive film. During evaporation, the crystal structure and stoichiometric ratio of $CsPbBr_3$ cannot be controlled uniformly, and some CsBr-rich and $PbBr_2$-rich domains will form because of thermally facilitated ion migration. Thus, even though raw $CsPbBr_3$ is highly crystalline, the deposited film is polycrystalline and contains several components.

Optical Materials EXPRESS

Currently, to achieve comparable or even higher performance from vacuum-evaporated LHP-LEDs with respect to the solution-processed device counterparts, the predominant challenge is a highly efficient LHP emissive film deposited using vacuum thermal evaporation. There are two main reasons that limit the light emitting efficiency of vacuum-evaporated LHP film. Firstly, the LHP crystal structure and even the ABX_3 stoichiometric ratio are destroyed during the thermal evaporation, and the resulting LHP emissive film deposited onto substrates are low-quality polycrystalline, which contains high density of defects. Therefore, obtaining a highly-crystalline LHP emissive film is essential. An in situ treatment, such as substrate heating, during the LHP film deposition could be helpful to improve their crystal quality. By virtue of ion migration of LHP, a post-treatment, including thermal annealing, solvent vapour annealing and using additives, can be used for healing defects of the deposited emissive film. However, these kinds of post-treatment steps will require to break vacuum, which trades off the advantage of vacuum-evaporated LHP-LEDs. Additionally, the substrate on which LHP film is deposited is also an important factor in determining the emissive film quality. Secondly, the low-efficiency light emission is determined by their delocalized charge carriers and slow bimolecular radiative recombination even in a vacuum-evaporated LHP single crystal. Based on the same idea of the solution-processed LHP-LEDs, a feasible scenario is the nanocrystallization of evaporated LHPs. The simultaneous co-evaporation of LHPs with a spacer could be a potential pathway to obtain monocrystalline LHPs, which is similar to the $CsPbBr_3/Cs_4PbBr_6$ composite structure (Fig. 3(d)) [125]. For selecting the spacer material, there are three requirements: First, the spacers should be a good evaporating material such as small molecular semiconductors. Second, the spacers should control the dimension of LHP grains deposited. And third, the spacers should passivate the LHP grain boundary defects.

In principle, solution-processed LHP-LEDs have a relative advantage in device fabrication cost because high vacuum is not essential for emissive LHP layer deposition. Until now, the performance of all-solution processed LHP-LEDs has still fallen behind their counterparts using hybrid film depositions of vacuum thermal evaporation and solution processing. However, it is worth emphasizing that one of the key features of vacuum-evaporated LHP-LEDs is their flexibility in device structure design, fabrication and optimization, especially for large-area applications. In this sense, an all-vacuum-evaporated LHP-LED is the most appropriate device which demonstrates this key feature. Although the solution-processed LHPs have made a breakthrough in large-area monochrome LEDs, the all-vacuum-evaporated LHP-LEDs will still play a predominant role in full color display requiring a highly uniform pattern of pixels. Moreover, all-evaporated LHP-LEDs in vacuum hardly output any toxic waste solution during manufacturing, which is more environmentally friendly and should be taken into consideration in terms of cost.

Disclosures. The authors declare no conflicts of interest.

Data availability. Data underlying the results presented in this paper are not publicly available at this time but may be obtained from the authors upon reasonable request.

References

1. L. Bai, S. Wang, Y. Zhang, K. Zhang, H. Li, K. Ou, and L. Yi, "Investigation on violet/blue all-inorganic light-emitting diodes based on $CsPbCl_3$ films," Journal of Luminescence **226**, 117422 (2020).
2. Y.-H. Kim, S. Kim, A. Kakekhani, J. Park, J. Park, Y.-H. Lee, H. Xu, S. Nagane, R. B. Wexler, D.-H. Kim, S. H. Jo, L. Martínez-Sarti, P. Tan, A. Sadhanala, G.-S. Park, Y.-W. Kim, B. Hu, H. J. Bolink, S. Yoo, R. H. Friend, A. M. Rappe, and T.-W. Lee, "Comprehensive defect suppression in perovskite nanocrystals for high-efficiency light-emitting diodes," Nat. Photonics **15**(2), 148–155 (2021).
3. K. Lin, J. Xing, L. N. Quan, F. P. G. de Arquer, X. Gong, J. Lu, L. Xie, W. Zhao, D. Zhang, C. Yan, W. Li, X. Liu, Y. Lu, J. Kirman, E. H. Sargent, Q. Xiong, and Z. Wei, "Perovskite light-emitting diodes with external quantum efficiency exceeding 20 per cent," Nature **562**(7726), 245–248 (2018).
4. J. Song, T. Fang, J. Li, L. Xu, F. Zhang, B. Han, Q. Shan, and H. Zeng, "Organic-inorganic hybrid passivation enables perovskite QLEDs with an EQE of 16.48," Adv. Mater. **30**, e1805409 (2018).

Optical Materials EXPRESS

5. B. Zhao, S. Bai, V. Kim, R. Lamboll, R. Shivanna, F. Auras, J. M. Richter, L. Yang, L. Dai, M. Alsari, X.-J. She, L. Liang, J. Zhang, S. Lilliu, P. Gao, H. J. Snaith, J. Wang, N. C. Greenham, R. H. Friend, and D. Di, "High-efficiency perovskite–polymer bulk heterostructure light-emitting diodes," Nat. Photonics **12**(12), 783–789 (2018).
6. F. Yan, J. Xing, G. Xing, L. Quan, S. T. Tan, J. Zhao, R. Su, L. Zhang, S. Chen, Y. Zhao, A. Huan, E. H. Sargent, Q. Xiong, and H. V. Demir, "Highly efficient visible colloidal lead-halide perovskite nanocrystal light-emitting diodes," Nano Lett. **18**(5), 3157–3164 (2018).
7. T. Chiba, Y. Hayashi, H. Ebe, K. Hoshi, J. Sato, S. Sato, Y.-J. Pu, S. Ohisa, and J. Kido, "Anion-exchange red perovskite quantum dots with ammonium iodine salts for highly efficient light-emitting devices," Nat. Photonics **12**(11), 681–687 (2018).
8. Z. Li, Z. Chen, Y. Yang, Q. Xue, H. L. Yip, and Y. Cao, "Modulation of recombination zone position for quasi-two-dimensional blue perovskite light-emitting diodes with efficiency exceeding 5," Nat. Commun. **10**(1), 1027 (2019).
9. L. Zhao, K. Roh, S. Kacmoli, K. Al Kurdi, S. Jhulki, S. Barlow, S. R. Marder, C. Gmachl, and B. P. Rand, "Thermal management enables bright and stable perovskite light-emitting diodes," Adv. Mater. **32**, e2000752 (2020).
10. Y. K. Wang, D. Ma, F. Yuan, K. Singh, J. M. Pina, A. Johnston, Y. Dong, C. Zhou, B. Chen, B. Sun, H. Ebe, J. Fan, M. J. Sun, Y. Gao, Z. H. Lu, O. Voznyy, L. S. Liao, and E. H. Sargent, "Chelating-agent-assisted control of $CsPbBr_3$ quantum well growth enables stable blue perovskite emitters," Nat. Commun. **11**(1), 3674 (2020).
11. X. Du, G. Wu, J. Cheng, H. Dang, K. Ma, Y.-W. Zhang, P.-F. Tan, and S. Chen, "High-quality $CsPbBr_3$ perovskite nanocrystals for quantum dot light-emitting diodes," RSC Adv. **7**(17), 10391–10396 (2017).
12. W. Cai, Z. Chen, D. Chen, S. Su, Q. Xu, H.-L. Yip, and Y. Cao, "High-performance and stable $CsPbBr_3$ light-emitting diodes based on polymer additive treatment," RSC Adv. **9**(47), 27684–27691 (2019).
13. Y. Sun, L. Zhang, N. Wang, S. Zhang, Y. Cao, Y. Miao, M. Xu, H. Zhang, H. Li, C. Yi, J. Wang, and W. Huang, "The formation of perovskite multiple quantum well structures for high performance light-emitting diodes," NPJ Flex Electron **2**(1), 12 (2018).
14. N. Wang, L. Cheng, R. Ge, S. Zhang, Y. Miao, W. Zou, C. Yi, Y. Sun, Y. Cao, R. Yang, Y. Wei, Q. Guo, Y. Ke, M. Yu, Y. Jin, Y. Liu, Q. Ding, D. Di, L. Yang, G. Xing, H. Tian, C. Jin, F. Gao, R. H. Friend, J. Wang, and W. Huang, "Perovskite light-emitting diodes based on solution-processed self-organized multiple quantum wells," Nat. Photonics **10**(11), 699–704 (2016).
15. Z. Ren, J. Yu, Z. Qin, J. Wang, J. Sun, C. C. S. Chan, S. Ding, K. Wang, R. Chen, K. S. Wong, X. Lu, W. J. Yin, and W. C. H. Choy, "High-performance blue perovskite light-emitting diodes enabled by efficient energy transfer between coupled quasi-2d perovskite layers," Adv. Mater. **33**, e2005570 (2021).
16. Y. J. Yoon, Y. S. Shin, H. Jang, J. G. Son, J. W. Kim, C. B. Park, D. Yuk, J. Seo, G. H. Kim, and J. Y. Kim, "Highly stable bulk perovskite for blue LEDs with anion-exchange method," Nano Lett. **21**(8), 3473–3479 (2021).
17. J. Xing, Y. Zhao, M. Askerka, L. N. Quan, X. Gong, W. Zhao, J. Zhao, H. Tan, G. Long, L. Gao, Z. Yang, O. Voznyy, J. Tang, Z. H. Lu, Q. Xiong, and E. H. Sargent, "Color-stable highly luminescent sky-blue perovskite light-emitting diodes," Nat. Commun. **9**(1), 3541 (2018).
18. F. Yan, S. T. Tan, X. Li, and H. V. Demir, "Light generation in lead halide perovskite nanocrystals: LEDs, color converters, lasers, and other applications," Small **15**, e1902079 (2019).
19. F. Yan and H. V. Demir, "LEDs using halide perovskite nanocrystal emitters," Nanoscale **11**(24), 11402–11412 (2019).
20. A. Dey, J. Ye, A. De, E. Debroye, S. K. Ha, E. Bladt, A. S. Kshirsagar, Z. Wang, J. Yin, Y. Wang, L. N. Quan, F. Yan, M. Gao, X. Li, J. Shamsi, T. Debnath, M. Cao, M. A. Scheel, S. Kumar, J. A. Steele, M. Gerhard, L. Chouhan, K. Xu, X. G. Wu, Y. Li, Y. Zhang, A. Dutta, C. Han, I. Vincon, A. L. Rogach, A. Nag, A. Samanta, B. A. Korgel, C. J. Shih, D. R. Gamelin, D. H. Son, H. Zeng, H. Zhong, H. Sun, H. V. Demir, I. G. Scheblykin, I. Mora-Sero, J. K. Stolarczyk, J. Z. Zhang, J. Feldmann, J. Hofkens, J. M. Luther, J. Perez-Prieto, L. Li, L. Manna, M. I. Bodnarchuk, M. V. Kovalenko, M. B. J. Roeffaers, N. Pradhan, O. F. Mohammed, O. M. Bakr, P. Yang, P. Muller-Buschbaum, P. V. Kamat, Q. Bao, Q. Zhang, R. Krahne, R. E. Galian, S. D. Stranks, S. Bals, V. Biju, W. A. Tisdale, Y. Yan, R. L. Z. Hoye, and L. Polavarapu, "State of the art and prospects for halide perovskite nanocrystals," ACS Nano **15**(7), 10775–10981 (2021).
21. Z. Liu, C. H. Lin, B. R. Hyun, C. W. Sher, Z. Lv, B. Luo, F. Jiang, T. Wu, C. H. Ho, H. C. Kuo, and J. H. He, "Micro-light-emitting diodes with quantum dots in display technology," Light Sci. Appl. **9**(1), 83 (2020).
22. T. Fang, T. Wang, X. Li, Y. Dong, S. Bai, and J. Song, "Perovskite QLED with an external quantum efficiency of over 21% by modulating electronic transport," Science Bulletin **66**(1), 36–43 (2021).
23. X. Dai, Z. Zhang, Y. Jin, Y. Niu, H. Cao, X. Liang, L. Chen, J. Wang, and X. Peng, "Solution-processed, high-performance light-emitting diodes based on quantum dots," Nature **515**(7525), 96–99 (2014).
24. C. Newby, J.-K. Lee, and C. K. Ober, "The solvent problem: Redissolution of macromolecules in solution-processed organic electronics," Macromol. Res. **21**(3), 248–256 (2013).
25. Y. Wei, J. Yu, L. Qin, H. Chen, X. Wu, Z. Wei, X. Zhang, Z. Xiao, L. Ding, F. Gao, and H. Huang, "A universal method for constructing high efficiency organic solar cells with stacked structures," Energy Environ. Sci. **14**(4), 2314–2321 (2021).
26. S. Ho, S. Liu, Y. Chen, and F. So, "Review of recent progress in multilayer solution-processed organic light-emitting diodes," J. Photon. Energy **5**(1), 057611 (2015).

Optical Materials EXPRESS

27. S. P. Senanayak, M. Abdi-Jalebi, V. S. Kamboj, R. Carey, R. Shivanna, T. Tian, G. Schweicher, J. Wang, N. Giesbrecht, D. Di Nuzzo, H. E. Beere, P. Docampo, D. A. Ritchie, D. Fairen-Jimenez, R. H. Friend, and H. Sirringhaus, "A general approach for hysteresis-free, operationally stable metal halide perovskite field-effect transistors," Sci. Adv. **6**(15), eaaz4948 (2020).
28. Y. Hu, Q. Wang, Y.-L. Shi, M. Li, L. Zhang, Z.-K. Wang, and L.-S. Liao, "Vacuum-evaporated all-inorganic cesium lead bromine perovskites for high-performance light-emitting diodes," J. Mater. Chem. C **5**(32), 8144–8149 (2017).
29. Y. Fu, Q. Zhang, D. Zhang, Y. Tang, L. Shu, Y. Zhu, and Z. Fan, "Scalable all-evaporation fabrication of efficient light-emitting diodes with hybrid 2D–3D perovskite nanostructures," Adv. Funct. Mater. **30**, 2002913 (2020).
30. X. Lian, X. Wang, Y. Ling, E. Lochner, L. Tan, Y. Zhou, B. Ma, K. Hanson, and H. Gao, "Light emitting diodes based on inorganic composite halide perovskites," Adv. Funct. Mater. **29**, 1807345 (2018).
31. Y. H. Song, S. H. Choi, W. K. Park, J. S. Yoo, S. B. Kwon, B. K. Kang, S. R. Park, Y. S. Seo, W. S. Yang, and D. H. Yoon, "Innovatively continuous mass production Couette-Taylor flow: pure inorganic green-emitting Cs_4PbBr_6 perovskite microcrystal for display technology," Sci. Rep. **8**(1), 2009 (2018).
32. J. Li, P. Du, S. Li, J. Liu, M. Zhu, Z. Tan, M. Hu, J. Luo, D. Guo, L. Ma, Z. Nie, Y. Ma, L. Gao, G. Niu, and J. Tang, "High-throughput combinatorial optimizations of perovskite light-emitting diodes based on all-vacuum deposition," Adv. Funct. Mater. **29**, 1903607 (2019).
33. S. Xie, A. Osherov, and V. Bulović, "All-vacuum-deposited inorganic cesium lead halide perovskite light-emitting diodes," APL Materials **8**(5), 051113 (2020).
34. L. Nasi, D. Calestani, F. Mezzadri, F. Mariano, A. Listorti, P. Ferro, M. Mazzeo, and R. Mosca, "All-Inorganic $CsPbBr_3$ perovskite films prepared by single source thermal ablation," Front. Chem. **8**, 313 (2020).
35. Z. Shangguan, X. Zheng, J. Zhang, W. Lin, W. Guo, C. Li, T. Wu, Y. Lin, and Z. Chen, "The stability of metal halide perovskite nanocrystals-a key issue for the application on quantum-dot-based micro light-emitting diodes display," Nanomaterials **10**(7), 1375 (2020).
36. C. Zhang, J. F. S. Fernando, K. L. Firestein, J. E. von Treifeldt, D. Siriwardena, X. Fang, and D. Golberg, "Thermal stability of $CsPbBr_3$ perovskite as revealed by in situ transmission electron microscopy," APL Materials **7**(7), 071110 (2019).
37. B. W. Boote, H. P. Andaraarachchi, B. A. Rosales, R. Blome-Fernandez, F. Zhu, M. D. Reichert, K. Santra, J. Li, J. W. Petrich, J. Vela, and E. A. Smith, "Unveiling the photo- and thermal-stability of cesium lead halide perovskite nanocrystals," ChemPhysChem **20**, 2647–2656 (2019).
38. L. Song, L. Huang, Y. Liu, X. Guo, C. Geng, S. Xu, Y. Xia, Y. Zhang, N. Luan, and Y. Hu, "Efficient thermally evaporated perovskite light-emitting devices via a bilateral interface engineering strategy," J. Phys. Chem. Lett. **12**(26), 6165–6173 (2021).
39. P. Du, J. Li, L. Wang, L. Sun, X. Wang, X. Xu, L. Yang, J. Pang, W. Liang, J. Luo, Y. Ma, and J. Tang, "Efficient and large-area all vacuum-deposited perovskite light-emitting diodes via spatial confinement," Nat. Commun. **12**(1), 4751 (2021).
40. K. Sim, T. Jun, J. Bang, H. Kamioka, J. Kim, H. Hiramatsu, and H. Hosono, "Performance boosting strategy for perovskite light-emitting diodes," Appl. Phys. Rev. **6**(3), 031402 (2019).
41. S. Chu, W. Chen, Z. Fang, X. Xiao, Y. Liu, J. Chen, J. Huang, and Z. Xiao, "Large-area and efficient perovskite light-emitting diodes via low-temperature blade-coating," Nat. Commun. **12**(1), 147 (2021).
42. F. Liu, Y. Zhang, C. Ding, S. Kobayashi, T. Izuishi, N. Nakazawa, T. Toyoda, T. Ohta, S. Hayase, T. Minemoto, K. Yoshino, S. Dai, and Q. Shen, "Highly luminescent phase-stable $CsPbI_3$ perovskite quantum dots achieving near 100% absolute photoluminescence quantum yield," ACS Nano **11**(10), 10373–10383 (2017).
43. H. Huang, L. Polavarapu, J. A. Sichert, A. S. Susha, A. S. Urban, and A. L. Rogach, "Colloidal lead halide perovskite nanocrystals: synthesis, optical properties and applications," NPG Asia Mater **8**(11), e328 (2016).
44. J. A. Sichert, Y. Tong, N. Mutz, M. Vollmer, S. Fischer, K. Z. Milowska, R. Garcia Cortadella, B. Nickel, C. Cardenas-Daw, J. K. Stolarczyk, A. S. Urban, and J. Feldmann, "Quantum size effect in organometal halide perovskite nanoplatelets," Nano Lett. **15**(10), 6521–6527 (2015).
45. Y. Bekenstein, B. A. Koscher, S. W. Eaton, P. Yang, and A. P. Alivisatos, "Highly luminescent colloidal nanoplates of perovskite cesium lead halide and their oriented assemblies," J. Am. Chem. Soc. **137**(51), 16008–16011 (2015).
46. S. Wang, C. Bi, J. Yuan, L. Zhang, and J. Tian, "Original core–shell structure of cubic $CsPbBr_3$@amorphous $CsPbBr_x$ perovskite quantum dots with a high blue photoluminescence quantum Yield of over 80%," ACS Energy Lett. **3**(1), 245–251 (2017).
47. X. Wu, M. T. Trinh, D. Niesner, H. Zhu, Z. Norman, J. S. Owen, O. Yaffe, B. J. Kudisch, and X. Y. Zhu, "Trap states in lead iodide perovskites," J. Am. Chem. Soc. **137**(5), 2089–2096 (2015).
48. L. Zhang, F. Yuan, H. Dong, B. Jiao, W. Zhang, X. Hou, S. Wang, Q. Gong, and Z. Wu, "One-step co-evaporation of all-inorganic perovskite thin films with room-temperature ultralow amplified spontaneous emission threshold and air stability," ACS Appl. Mater. Interfaces **10**(47), 40661–40671 (2018).
49. B. Philippe, T. J. Jacobsson, J.-P. Correa-Baena, N. K. Jena, A. Banerjee, S. Chakraborty, U. B. Cappel, R. Ahuja, A. Hagfeldt, M. Odelius, and H. Rensmo, "Valence level character in a mixed perovskite material and determination of the valence band maximum from photoelectron spectroscopy: variation with photon energy," J. Phys. Chem. C **121**(48), 26655–26666 (2017).
50. M. V. Kovalenko, L. Protesescu, and M. I. Bodnarchuk, "Properties and potential optoelectronic applications of lead halide perovskite nanocrystals," Science **358**(6364), 745–750 (2017).

Optical Materials EXPRESS

51. A. D. Wright, C. Verdi, R. L. Milot, G. E. Eperon, M. A. Perez-Osorio, H. J. Snaith, F. Giustino, M. B. Johnston, and L. M. Herz, "Electron-phonon coupling in hybrid lead halide perovskites," Nat. Commun. **7**(1), 11755 (2016).
52. J. Kang and L. W. Wang, "High defect tolerance in lead halide perovskite $CsPbBr_3$," J. Phys. Chem. Lett. **8**(2), 489–493 (2017).
53. J. S. Manser, J. A. Christians, and P. V. Kamat, "Intriguing optoelectronic properties of metal halide perovskites," Chem. Rev. **116**(21), 12956–13008 (2016).
54. S. Meloni, G. Palermo, N. Ashari-Astani, M. Grätzel, and U. Rothlisberger, "Valence and conduction band tuning in halide perovskites for solar cell applications," J. Mater. Chem. A **4**(41), 15997–16002 (2016).
55. L. Protesescu, S. Yakunin, M. I. Bodnarchuk, F. Krieg, R. Caputo, C. H. Hendon, R. X. Yang, A. Walsh, and M. V. Kovalenko, "Nanocrystals of cesium lead halide perovskites ($CsPbX_{(3)}$, X = Cl, Br, and I): novel optoelectronic materials showing bright emission with wide color gamut," Nano Lett. **15**(6), 3692–3696 (2015).
56. S. Tao, I. Schmidt, G. Brocks, J. Jiang, I. Tranca, K. Meerholz, and S. Olthof, "Absolute energy level positions in tin- and lead-based halide perovskites," Nat. Commun. **10**(1), 2560 (2019).
57. J. Ahn, Y. M. Lee, W. Kim, and S. J. Oh, "Cation effect on anion exchange in $CsPbX_3$ (X = Cl, Br, I) perovskite nanocrystals," ECS Trans. **102**(1), 75–82 (2021).
58. J. Xing, F. Yan, Y. Zhao, S. Chen, H. Yu, Q. Zhang, R. Zeng, H. V. Demir, X. Sun, A. Huan, and Q. Xiong, "High-efficiency light-emitting diodes of organometal halide perovskite amorphous nanoparticles," ACS Nano **10**(7), 6623–6630 (2016).
59. A. Sadhanala, S. Ahmad, B. Zhao, N. Giesbrecht, P. M. Pearce, F. Deschler, R. L. Hoye, K. C. Godel, T. Bein, P. Docampo, S. E. Dutton, M. F. De Volder, and R. H. Friend, "Blue-green color tunable solution processable organolead chloride-bromide mixed halide perovskites for optoelectronic applications," Nano Lett. **15**(9), 6095–6101 (2015).
60. W. Tress, "Metal halide perovskites as mixed electronic-ionic conductors: challenges and opportunities-from hysteresis to memristivity," J. Phys. Chem. Lett. **8**(13), 3106–3114 (2017).
61. Y. H. Ko, M. Jalalah, S. J. Lee, and J. G. Park, "Super ultra-high resolution liquid-crystal-display using perovskite quantum-dot functional color-filters," Sci Rep **8**(1), 12881 (2018).
62. H. C. Yoon, H. Lee, H. Kang, J. H. Oh, and Y. R. Do, "Highly efficient wide-color-gamut QD-emissive LCDs using red and green perovskite core/shell QDs," J. Mater. Chem. C **6**(47), 13023–13033 (2018).
63. Y. H. Kim, H. Cho, and T. W. Lee, "Metal halide perovskite light emitters," Proc. Natl. Acad. Sci. U S A **113**(42), 11694–11702 (2016).
64. J. A. Steele, P. Puech, M. Keshavarz, R. Yang, S. Banerjee, E. Debroye, C. W. Kim, H. Yuan, N. H. Heo, J. Vanacken, A. Walsh, J. Hofkens, and M. B. J. Roeffaers, "Giant electron-phonon coupling and deep conduction band resonance in metal halide double perovskite," ACS Nano **12**(8), 8081–8090 (2018).
65. Q. A. Akkerman, G. Raino, M. V. Kovalenko, and L. Manna, "Genesis, challenges and opportunities for colloidal lead halide perovskite nanocrystals," Nature Mater **17**(5), 394–405 (2018).
66. M. A. Becker, R. Vaxenburg, G. Nedelcu, P. C. Sercel, A. Shabaev, M. J. Mehl, J. G. Michopoulos, S. G. Lambrakos, N. Bernstein, J. L. Lyons, T. Stoferle, R. F. Mahrt, M. V. Kovalenko, D. J. Norris, G. Raino, and A. L. Efros, "Bright triplet excitons in caesium lead halide perovskites," Nature **553**(7687), 189–193 (2018).
67. G. Tang, P. Ghosez, and J. Hong, "Band-edge orbital engineering of perovskite semiconductors for optoelectronic applications," J. Phys. Chem. Lett. **12**(17), 4227–4239 (2021).
68. G. W. Kim and A. Petrozza, "Defect tolerance and intolerance in metal-halide perovskites," Adv. Energy Mater. **10**, 2001959 (2020).
69. S. C. Liu, C. M. Dai, Y. Min, Y. Hou, A. H. Proppe, Y. Zhou, C. Chen, S. Chen, J. Tang, D. J. Xue, E. H. Sargent, and J. S. Hu, "An antibonding valence band maximum enables defect-tolerant and stable GeSe photovoltaics," Nat. Commun. **12**(1), 670 (2021).
70. H. Huang, M. I. Bodnarchuk, S. V. Kershaw, M. V. Kovalenko, and A. L. Rogach, "Lead halide perovskite nanocrystals in the research spotlight: stability and defect tolerance," ACS Energy Lett. **2**(9), 2071–2083 (2017).
71. M. Pandey, K. W. Jacobsen, and K. S. Thygesen, "Band gap tuning and defect tolerance of atomically thin two-dimensional organic-inorganic halide perovskites," J. Phys. Chem. Lett. **7**(21), 4346–4352 (2016).
72. C. Li, A. Guerrero, S. Huettner, and J. Bisquert, "Unravelling the role of vacancies in lead halide perovskite through electrical switching of photoluminescence," Nat. Commun. **9**(1), 5113 (2018).
73. Y. Zhou, I. Poli, D. Meggiolaro, F. De Angelis, and A. Petrozza, "Defect activity in metal halide perovskites with wide and narrow bandgap," Nat Rev Mater **6**(11), 986–1002 (2021).
74. K. Jia, L. Song, Y. Hu, X. Guo, X. Liu, C. Geng, S. Xu, R. Fan, L. Huang, N. Luan, and W. Bi, "Improved performance for thermally evaporated perovskite light-emitting devices via defect passivation and carrier regulation," ACS Appl. Mater. Interfaces **12**(13), 15928–15933 (2020).
75. G. Xing, B. Wu, X. Wu, M. Li, B. Du, Q. Wei, J. Guo, E. K. Yeow, T. C. Sum, and W. Huang, "Transcending the slow bimolecular recombination in lead-halide perovskites for electroluminescence," Nat. Commun. **8**(1), 14558 (2017).
76. G. Longo, L. Gil-Escrig, M. J. Degen, M. Sessolo, and H. J. Bolink, "Perovskite solar cells prepared by flash evaporation," Chem. Commun. **51**(34), 7376–7378 (2015).
77. M. Baranowski and P. Plochocka, "Excitons in metal-halide perovskites," Adv. Energy Mater. **10**(26), 1903659 (2020).

Optical Materials EXPRESS

78. M. Hu, C. Bi, Y. Yuan, Z. Xiao, Q. Dong, Y. Shao, and J. Huang, "Distinct exciton dissociation behavior of organolead trihalide perovskite and excitonic semiconductors studied in the same system," Small **11**, 2164–2169 (2015).
79. A. Jha, H.-G. Duan, V. Tiwari, P. K. Nayak, H. J. Snaith, M. Thorwart, and R. J. D. Miller, "Direct observation of ultrafast exciton dissociation in lead iodide perovskite by 2D electronic spectroscopy," ACS Photonics **5**(3), 852–860 (2017).
80. C. L. Davies, M. R. Filip, J. B. Patel, T. W. Crothers, C. Verdi, A. D. Wright, R. L. Milot, F. Giustino, M. B. Johnston, and L. M. Herz, "Bimolecular recombination in methylammonium lead triiodide perovskite is an inverse absorption process," Nat. Commun. **9**(1), 293 (2018).
81. F. Ambrosio, J. Wiktor, F. De Angelis, and A. Pasquarello, "Origin of low electron–hole recombination rate in metal halide perovskites," Energy Environ. Sci. **11**(1), 101–105 (2018).
82. T. S. Sherkar, C. Momblona, L. Gil-Escrig, J. Avila, M. Sessolo, H. J. Bolink, and L. J. A. Koster, "Recombination in perovskite solar cells: significance of grain boundaries, interface traps, and defect ions," ACS Energy Lett. **2**(5), 1214–1222 (2017).
83. V. Kattoor, K. Awasthi, E. Jokar, E. W. Diau, and N. Ohta, "Enhanced dissociation of hot excitons with an applied electric field under low-power photoexcitation in two-dimensional perovskite quantum wells," J. Phys. Chem. Lett. **10**(16), 4752–4757 (2019).
84. R. Saraf and V. Maheshwari, "Self-powered photodetector based on electric-field-induced effects in $MAPbI_3$ perovskite with improved stability," ACS Appl. Mater. Interfaces **10**(25), 21066–21072 (2018).
85. S.-H. Turren-Cruz, M. Saliba, M. T. Mayer, H. Juárez-Santiesteban, X. Mathew, L. Nienhaus, W. Tress, M. P. Erodici, M.-J. Sher, M. G. Bawendi, M. Grätzel, A. Abate, A. Hagfeldt, and J.-P. Correa-Baena, "Enhanced charge carrier mobility and lifetime suppress hysteresis and improve efficiency in planar perovskite solar cells," Energy Environ. Sci. **11**(1), 78–86 (2018).
86. N. D. Canicoba, N. Zagni, F. Liu, G. McCuistian, K. Fernando, H. Bellezza, B. Traoré, R. Rogel, H. Tsai, L. Le Brizoual, W. Nie, J. J. Crochet, S. Tretiak, C. Katan, J. Even, M. G. Kanatzidis, B. W. Alphenaar, J.-C. Blancon, M. A. Alam, and A. D. Mohite, "Halide perovskite high-k field effect transistors with dynamically reconfigurable ambipolarity," ACS Materials Lett. **1**(6), 633–640 (2019).
87. A. Younis, C. H. Lin, X. Guan, S. Shahrokhi, C. Y. Huang, Y. Wang, T. He, S. Singh, L. Hu, J. R. D. Retamal, J. H. He, and T. Wu, "Halide Perovskites: a new era of solution-processed electronics," Adv. Mater. **33**(23), e2005000 (2021).
88. K. Miyata, D. Meggiolaro, M. T. Trinh, P. P. Joshi, E. Mosconi, S. C. Jones, F. De Angelis, and X. Y. Zhu, "Large polarons in lead halide perovskites," Sci. Adv. **3**(8), e1701217 (2017).
89. J. M. Frost, "Calculating polaron mobility in halide perovskites," Phys. Rev. B **96**(19), 195202 (2017).
90. L. M. Herz, "Charge-carrier mobilities in metal halide perovskites: fundamental mechanisms and limits," ACS Energy Lett. **2**(7), 1539–1548 (2017).
91. G. Xing, N. Mathews, S. Sun, S. S. Lim, Y. M. Lam, M. Gratzel, S. Mhaisalkar, and T. C. Sum, "Long-range balanced electron- and hole-transport lengths in organic-inorganic $CH_3NH_3PbI_3$," Science **342**(6156), 344–347 (2013).
92. Q. Dong, J. Mendes, L. Lei, D. Seyitliyev, L. Zhu, S. He, K. Gundogdu, and F. So, "Understanding the role of ion migration in the operation of perovskite light-emitting diodes by transient measurements," ACS Appl. Mater. Interfaces **12**(43), 48845–48853 (2020).
93. S. Ghosh, S. K. Pal, K. J. Karki, and T. Pullerits, "Ion migration heals trapping centers in $CH_3NH_3PbBr_3$ perovskite," ACS Energy Lett. **2**(9), 2133–2139 (2017).
94. W. Nie, J. C. Blancon, A. J. Neukirch, K. Appavoo, H. Tsai, M. Chhowalla, M. A. Alam, M. Y. Sfeir, C. Katan, J. Even, S. Tretiak, J. J. Crochet, G. Gupta, and A. D. Mohite, "Light-activated photocurrent degradation and self-healing in perovskite solar cells," Nat. Commun. **7**(1), 11574 (2016).
95. T. Zhang, M. Long, K. Yan, M. Qin, X. Lu, X. Zeng, C. M. Cheng, K. S. Wong, P. Liu, W. Xie, and J. Xu, "Crystallinity preservation and ion migration suppression through dual ion exchange strategy for stable mixed perovskite solar cells," Adv. Energy Mater. **7**(15), 1700118 (2017).
96. L. Zhang, F. Yuan, J. Xi, B. Jiao, H. Dong, J. Li, and Z. Wu, "Suppressing ion migration enables stable perovskite light-emitting diodes with all-inorganic strategy," Adv. Funct. Mater. **30**(40), 2001834 (2020).
97. N. Li, L. Song, Y. Jia, Y. Dong, F. Xie, L. Wang, S. Tao, and N. Zhao, "Stabilizing perovskite light-emitting diodes by incorporation of binary alkali cations," Adv. Mater. **32**(17), e1907786 (2020).
98. F. Di Stasio, S. Christodoulou, N. Huo, and G. Konstantatos, "Near-unity photoluminescence quantum yield in cspbbr3 nanocrystal solid-state films via postsynthesis treatment with lead bromide," Chem. Mater. **29**(18), 7663–7667 (2017).
99. M. Ross, L. Gil-Escrig, A. Al-Ashouri, P. Tockhorn, M. Jost, B. Rech, and S. Albrecht, "Co-evaporated p-i-n perovskite solar cells beyond 20% efficiency: impact of substrate temperature and hole-transport layer," ACS Appl. Mater. Interfaces **12**(35), 39261–39272 (2020).
100. Z. H. Zheng, H. B. Lan, Z. H. Su, H. X. Peng, J. T. Luo, G. X. Liang, and P. Fan, "Single source thermal evaporation of two-dimensional perovskite thin films for photovoltaic applications," Sci Rep **9**(1), 17422 (2019).

Optical Materials EXPRESS

101. J. M. Ball, L. Buizza, H. C. Sansom, M. D. Farrar, M. T. Klug, J. Borchert, J. Patel, L. M. Herz, M. B. Johnston, and H. J. Snaith, "Dual-source coevaporation of low-bandgap $FA_{1-x}Cs_xSn_{1-y}Pb_yI_3$ perovskites for photovoltaics," ACS Energy Lett. **4**(11), 2748–2756 (2019).
102. Y. Yu, D. Zhao, C. R. Grice, W. Meng, C. Wang, W. Liao, A. J. Cimaroli, H. Zhang, K. Zhu, and Y. Yan, "Thermally evaporated methylammonium tin triiodide thin films for lead-free perovskite solar cell fabrication," RSC Adv. **6**(93), 90248–90254 (2016).
103. J. A. Schwenzer, T. Hellmann, B. A. Nejand, H. Hu, T. Abzieher, F. Schackmar, I. M. Hossain, P. Fassl, T. Mayer, W. Jaegermann, U. Lemmer, and U. W. Paetzold, "Thermal stability and cation composition of hybrid organic-inorganic perovskites," ACS Appl. Mater. Interfaces **13**(13), 15292–15304 (2021).
104. M. Wang, V. Vasudevan, S. Lin, J. Jasieniak, S. P. Russo, N. Birbilis, and N. V. Medhekar, "Molecular mechanisms of thermal instability in hybrid perovskite light absorbers for photovoltaic solar cells," J. Mater. Chem. A **8**(34), 17765–17779 (2020).
105. D. Calestani, L. Nasi, F. Mezzadri, F. Fracassi, A. Listorti, P. Ferro, and R. Mosca, "Single-source thermal ablation of halide perovskites, limitations and opportunities: the lesson of $MAPbBr_3$," Journal of Alloys and Compounds **875**(10), 159954 (2021).
106. A. Dualeh, P. Gao, S. I. Seok, M. K. Nazeeruddin, and M. Grätzel, "Thermal behavior of methylammonium lead-trihalide perovskite photovoltaic light harvesters," Chem. Mater. **26**(21), 6160–6164 (2014).
107. R. Swartwout, M. T. Hoerantner, and V. Bulović, "Scalable deposition methods for large-area production of perovskite thin films," Energy Environ. Mater. **2**(2), 119–145 (2019).
108. J. Li, R. Gao, F. Gao, J. Lei, H. Wang, X. Wu, J. Li, H. Liu, X. Hua, and S. Liu, "Fabrication of efficient $CsPbBr_3$ perovskite solar cells by single-source thermal evaporation," Journal of Alloys and Compounds **818**, 152903 (2020).
109. S. Bai, P. Da, C. Li, Z. Wang, Z. Yuan, F. Fu, M. Kawecki, X. Liu, N. Sakai, J. T. Wang, S. Huettner, S. Buecheler, M. Fahlman, F. Gao, and H. J. Snaith, "Planar perovskite solar cells with long-term stability using ionic liquid additives," Nature **571**(7764), 245–250 (2019).
110. G. Li, Z. Su, M. Li, F. Yang, M. H. Aldamasy, J. Pascual, F. Yang, H. Liu, W. Zuo, D. D. Girolamo, Z. Iqbal, G. Nasti, A. Dallmann, X. Gao, Z. Wang, M. Saliba, and A. Abate, "Ionic liquid stabilizing high-efficiency tin halide perovskite solar cells," Adv. Energy Mater. **11**(32), 2101539 (2021).
111. J. Yin, P. Maity, M. De Bastiani, I. Dursun, O. M. Bakr, J. L. Bredas, and O. F. Mohammed, "Molecular behavior of zero-dimensional perovskites," Sci. Adv. **3**(12), e1701793 (2017).
112. C.-G. Park, W.-G. Choi, S. Na, and T. Moon, "All-inorganic perovskite $CsPbI_2Br$ through co-evaporation for planar heterojunction solar cells," Electron. Mater. Lett. **15**(1), 56–60 (2018).
113. J. C. Dahl, X. Wang, X. Huang, E. M. Chan, and A. P. Alivisatos, "Elucidating the weakly reversible cs-Pb-Br perovskite nanocrystal reaction network with high-throughput maps and transformations," J. Am. Chem. Soc. **142**(27), 11915–11926 (2020).
114. D. M. Jang, K. Park, D. H. Kim, J. Park, F. Shojaei, H. S. Kang, J. P. Ahn, J. W. Lee, and J. K. Song, "Reversible halide exchange reaction of organometal trihalide perovskite colloidal nanocrystals for full-range band gap tuning," Nano Lett. **15**(8), 5191–5199 (2015).
115. B. T. Diroll, G. Nedelcu, M. V. Kovalenko, and R. D. Schaller, "High-temperature photoluminescence of $CsPbX_3$ (X = Cl, Br, I) nanocrystals," Adv. Funct. Mater. **27**, 1606750 (2017).
116. M. Liao, B. Shan, and M. Li, "In situ Raman spectroscopic studies of thermal stability of all-inorganic cesium lead halide ($CsPbX_3$, X = Cl, Br, I) perovskite nanocrystals," J. Phys. Chem. Lett. **10**(6), 1217–1225 (2019).
117. T. Burwig, W. Franzel, and P. Pistor, "Crystal phases and thermal stability of co-evaporated $CsPbX_3$ (X = I, Br) thin films," J. Phys. Chem. Lett. **9**(16), 4808–4813 (2018).
118. Y. Rakita, N. Kedem, S. Gupta, A. Sadhanala, V. Kalchenko, M. L. Böhm, M. Kulbak, R. H. Friend, D. Cahen, and G. Hodes, "Low-temperature solution-grown $CsPbBr_3$ single crystals and their characterization," Crystal Growth & Design **16**(10), 5717–5725 (2016).
119. C. Y. Chen, H. Y. Lin, K. M. Chiang, W. L. Tsai, Y. C. Huang, C. S. Tsao, and H. W. Lin, "All-vacuum-deposited stoichiometrically balanced inorganic cesium lead halide perovskite solar cells with stabilized efficiency exceeding 11," Adv. Mater. **29**(4), 1605290 (2017).
120. G. Tong, T. Chen, H. Li, L. Qiu, Z. Liu, Y. Dang, W. Song, L. K. Ono, Y. Jiang, and Y. Qi, "Phase transition induced recrystallization and low surface potential barrier leading to 10.91%-efficient CsPbBr3 perovskite solar cells," Nano Energy **65**, 104015 (2019).
121. K. B. Lohmann, J. B. Patel, M. U. Rothmann, C. Q. Xia, R. D. J. Oliver, L. M. Herz, H. J. Snaith, and M. B. Johnston, "Control over crystal size in vapor deposited metal-halide perovskite films," ACS Energy Lett. **5**(3), 710–717 (2020).
122. C. Bi, Q. Wang, Y. Shao, Y. Yuan, Z. Xiao, and J. Huang, "Non-wetting surface-driven high-aspect-ratio crystalline grain growth for efficient hybrid perovskite solar cells," Nat. Commun. **6**(1), 7747 (2015).
123. Y. H. Deng, Z. Q. Yang, and R. M. Ma, "Growth of centimeter-scale perovskite single-crystalline thin film via surface engineering," Nano Convergence **7**(1), 25 (2020).
124. H. Wang, M. Zhou, and H. Luo, "Electric-field-induced dynamic electronic junctions in hybrid organic-inorganic perovskites for optoelectronic applications," ACS Omega **3**(2), 1445–1450 (2018).
125. S. Chang, Z. Bai, and H. Zhong, "In situ fabricated perovskite nanocrystals: a revolution in optical materials," Adv. Opt. Mater. **6**, 1800380 (2018).

Optical Materials EXPRESS

126. C. Momblona, L. Gil-Escrig, E. Bandiello, E. M. Hutter, M. Sessolo, K. Lederer, J. Blochwitz-Nimoth, and H. J. Bolink, "Efficient vacuum deposited p-i-n and n-i-p perovskite solar cells employing doped charge transport layers," Energy Environ. Sci. **9**(11), 3456–3463 (2016).
127. L. Y. Bai, S. W. Wang, Y. W. Zhang, K. X. Zhang, and L. X. Yi, "Influence of annealing process on the stable luminous $CsPbCl_3$ perovskite films by thermal evaporation," Journal of Luminescence **227**, 117592 (2020).
128. C. Pu, X. Dai, Y. Shu, M. Zhu, Y. Deng, Y. Jin, and X. Peng, "Electrochemically-stable ligands bridge the photoluminescence-electroluminescence gap of quantum dots," Nat. Commun. **11**(1), 937 (2020).
129. Z. Li, K. Cao, J. Li, X. Du, Y. Tang, and B. Yu, "Modification of interface between PEDOT:PSS and perovskite film inserting an ultrathin LiF layer for enhancing efficiency of perovskite light-emitting diodes," Organic Electronics **81**, 105675 (2020).
130. J. C. Yu, J. A. Hong, E. D. Jung, D. B. Kim, S. M. Baek, S. Lee, S. Cho, S. S. Park, K. J. Choi, and M. H. Song, "Highly efficient and stable inverted perovskite solar cell employing PEDOT:GO composite layer as a hole transport layer," Sci Rep **8**(1), 1070 (2018).
131. C. Eames, J. M. Frost, P. R. Barnes, B. C. O'Regan, A. Walsh, and M. S. Islam, "Ionic transport in hybrid lead iodide perovskite solar cells," Nat. Commun. **6**(1), 7497 (2015).
132. X. Shan, J. Li, M. Chen, T. Geske, S. G. R. Bade, and Z. Yu, "Junction propagation in organometal halide perovskite-polymer composite thin films," J. Phys. Chem. Lett. **8**(11), 2412–2419 (2017).
133. Z. Bin, L. Duan, and Y. Qiu, "Air stable organic salt as an n-type dopant for efficient and stable organic light-emitting diodes," ACS Appl. Mater. Interfaces **7**(12), 6444–6450 (2015).
134. S. Reineke, F. Lindner, G. Schwartz, N. Seidler, K. Walzer, B. Lussem, and K. Leo, "White organic light-emitting diodes with fluorescent tube efficiency," Nature **459**(7244), 234–238 (2009).
135. I. W. Wu, C.-L. Chuang, P.-S. Wang, W.-H. Tseng, and C.-I. Wu, "The investigation of the diffusion length of cathode materials in organic light emitting devices through impedance characteristics," Appl. Phys. Lett. **100**(17), 173302 (2012).
136. B. Lüssem, M. Riede, and K. Leo, "Doping of organic semiconductors," Phys. Status Solidi A **210**(1), 9–43 (2013).
137. Y. Shang, Y. Liao, Q. Wei, Z. Wang, B. Xiang, Y. Ke, W. Liu, and Z. Ning, "Highly stable hybrid perovskite light-emitting diodes based on Dion-Jacobson structure," Sci. Adv. **5**(8), eaaw8072 (2019).
138. P. Lu, J. Wu, X. Shen, X. Gao, Z. Shi, M. Lu, W. W. Yu, and Y. Zhang, "ZnO-Ti_3C_2 MXene electron transport layer for high external quantum efficiency perovskite nanocrystal light-emitting diodes," Adv. Sci. **7**(19), 2001562 (2020).
139. Z. Yuan, Y. Miao, Z. Hu, W. Xu, C. Kuang, K. Pan, P. Liu, J. Lai, B. Sun, J. Wang, S. Bai, and F. Gao, "Unveiling the synergistic effect of precursor stoichiometry and interfacial reactions for perovskite light-emitting diodes," Nat. Commun. **10**(1), 2818 (2019).
140. H. Wang, H. Yu, W. Xu, Z. Yuan, Z. Yan, C. Wang, X. Liu, M. Fahlman, J. M. Liu, X. K. Liu, and F. Gao, "Efficient perovskite light-emitting diodes based on a solution-processed tin dioxide electron transport layer," J. Mater. Chem. C **6**(26), 6996–7002 (2018).
141. L. Zhang, X. Yang, Q. Jiang, P. Wang, Z. Yin, X. Zhang, H. Tan, Y. M. Yang, M. Wei, B. R. Sutherland, E. H. Sargent, and J. You, "Ultra-bright and highly efficient inorganic based perovskite light-emitting diodes," Nat. Commun. **8**(1), 15640 (2017).